photonics

MDPI

Article

Diffraction-Mediated Self-Structuring of a Bose–Einstein Condensate: Instability Threshold and Dynamics

Gordon R. M. Robb *, Kelsey O'Donnell, Gian-Luca Oppo and Thorsten Ackemann

Department of Physics, Scottish Universitites Physics Alliance (SUPA), University of Strathclyde, Glasgow G4 0NG, UK; kelsey.o-donnell@strath.ac.uk (K.O.); g.l.oppo@strath.ac.uk (G.-L.O.); thorsten.ackemann@strath.ac.uk (T.A.)

* Correspondence: g.r.m.robb@strath.ac.uk

Abstract

We study a 1D model of a diffraction-mediated self-structuring instability which can occur when a Bose–Einstein condensate is illuminated by a pump laser and its reflection from a single feedback mirror. We carry out a linear stability analysis and, using numerical simulations, investigate the dynamics of the self-structuring process. Two dynamical regimes are identified: one in which the system behaves as a continuous space-time crystal oscillating between two states (one spatially uniform and one spatially periodic) and another where many condensate momentum states are involved and the condensate density develops chevrons which form and disperse quasi-periodically. We show the dependence of the pattern modulation depth and pattern formation time on pump saturation parameter and compare the simulation results with analytical expressions derived from a quantum Hamiltonian Mean Field model. The results show that this system offers a route to the first experimental realisation of the quantum Hamiltonian Mean Field model and of a continuous space-time crystal with a tunable spatial period.

Keywords: optomechanics; Bose–Einstein condensate; pattern formation; self-organization

1. Introduction

Spontaneous, self-organised patterns produced via a combination of optical diffraction and nonlinearity have been predicted and observed in a range of media [1–10] including hot atomic vapours [1–6,11–13]. There has been significant recent interest in self-organizing behaviour involving cold thermal gases and Bose–Einstein Condensates (BECs) interacting with counterpropagating optical beams in free space [14,15] or with one or more modes of an optical cavity [16–21]. These studies have produced a wide range of interesting nonlinear and quantum phenomena, e.g., collective atomic recoil lasing (CARL) [16,22], Dicke superradiance [23] and supersolid formation [24–26]. In contrast to pattern formation in hot vapours, where the origin of the optical nonlinearity is electronic or magnetic internal atomic states, optical nonlinearity in cold thermal gases and BECs is due to centre-of-mass motion of the atoms under the mechanical action of light, specifically optical dipole forces. This optomechanical self-structuring has also been studied experimentally and theoretically for a cold thermal gas in a single mirror feedback (SMF) configuration [27,28], with diffraction of light providing spatial coupling between different parts of the atomic gas. The existence of an optomechanical self-structuring instability in a BEC was predicted in [29–31]. Here we present a derivation of the conditions under which an instability leading to optomechanical self-structuring in a BEC with SMF can occur and study the

Check for updates

Received: 16 February 2026
Revised: 6 April 2026
Accepted: 9 April 2026
Published: 22 April 2026

Copyright: © 2026 by the authors. Licensee MDPI, Basel, Switzerland. This article is an open access article distributed under the terms and conditions of the Creative Commons Attribution (CC BY) license.

dynamical behaviour of the BEC and optical fields produced by the instability in both real space and momentum space. The BEC-SMF system can be mapped onto the quantum Hamiltonian Mean Field (HMF) model and thus provides an experimental pathway to realise this archetypical model for long-range coupling in statistical physics [32].

2. Model

We investigate a system consisting of a BEC interacting with an optical field via a single mirror feedback (SMF) as shown schematically in Figure 1. In this BEC-SMF system, coupling between atoms arises due to diffraction of light, involves many transverse optical modes and optical forces directed perpendicular to the propagation direction of the optical fields.

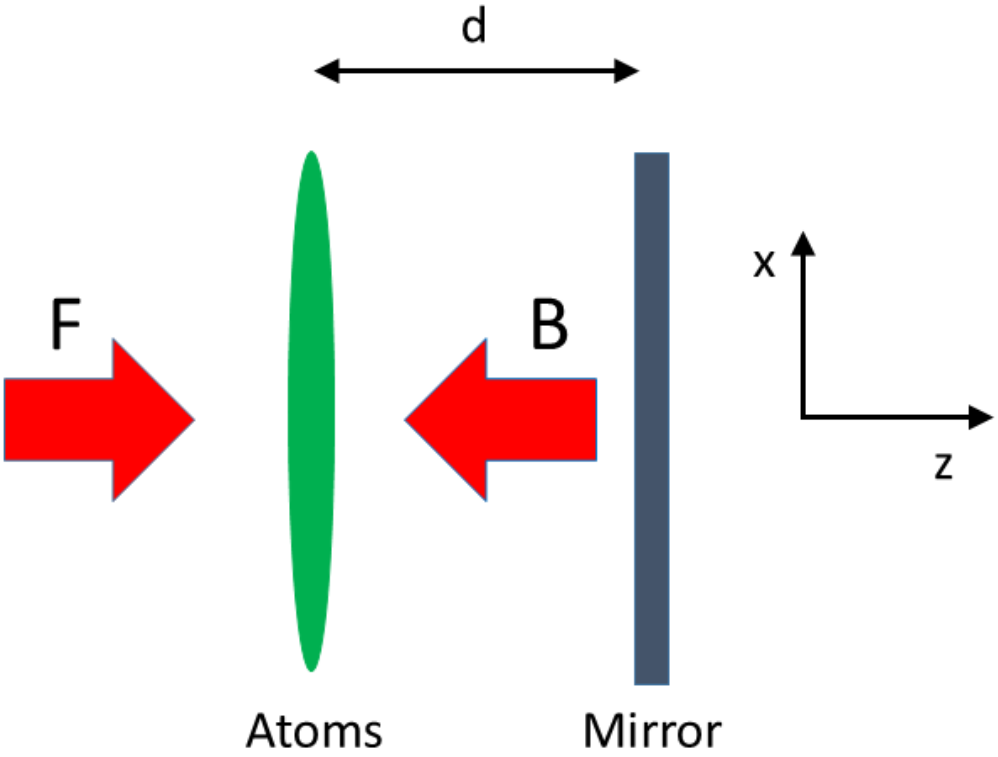


Figure 1. Schematic diagram of the single mirror feedback (SMF) configuration showing a BEC interacting with a forward propagating optical field (F) and a backward propagating optical field (B) reflected from a mirror of reflectivity, R, at a distance d from the BEC.

The model we use to describe the BEC-SMF system was originally studied in [29]. We consider a BEC with negligible atomic collisions and describe the evolution of the BEC wavefunction, $\Psi(\bar{x}, \bar{t})$ with the Schrödinger equation:

$$i\frac{\partial \Psi(\bar{x},\bar{t})}{\partial \bar{t}} = -\bar{\omega}_r \frac{\partial^2 \Psi}{\partial \bar{x}^2} + \frac{\Delta}{4}\left(|F|^2 + |B|^2\right)\Psi \tag{1}$$

where $\bar{t} = \Gamma t$ and $\bar{x} = q_c x$ are dimensionless time and space variables, $q_c = \sqrt{\frac{\pi k_0}{d}}$ is a critical transverse wavenumber, $k_0 = \frac{2\pi}{\lambda}$ and λ are the optical pump wavenumber and wavelength respectively, d is the distance from the BEC to the mirror, Γ is the decay rate of the atomic transition, $\bar{\omega}_r = \frac{\hbar q_c^2}{2m\Gamma}$ is a dimensionless recoil frequency, and m is the atomic mass. The variable $s(x,t) = |F|^2 + |B(x,t)|^2$ is the atomic saturation parameter due to the forward and backward optical fields where $|F|^2 = \frac{I_F}{I_{sat}\Delta^2}$, $|B|^2 = \frac{I_B}{I_{sat}\Delta^2}$, I_F, I_B are the intensities of the forward (F) and backward (B) fields respectively. I_{sat} is the saturation intensity on resonance, $\Delta = \frac{2\delta}{\Gamma}$ is a dimensionless detuning parameter where $\delta = \omega - \omega_a$ is

the difference between the optical field frequency, ω, and the atomic transition frequency, ω_a. It has been assumed that $|\Delta| \gg 1$ and that consequently $s \ll 1$ so that the atoms remain in their ground internal energy state. In addition, longitudinal grating effects due to interference between the counterpropagating optical fields are neglected. As we are primarily interested in the interaction between the BEC and the optical field, we neglect atomic collisions, effectively assuming negligible BEC scattering length.

In order to describe the optical field in the BEC we assume that the BEC is sufficiently thin that diffraction can be neglected, so that the forward field transmitted through it is

$$F^{tr} = \sqrt{p_0}\exp\left(-i\frac{b_0}{2\Delta}n(x,t)\right) \tag{2}$$

where $p_0 = |F(z=0)|^2$ is the scaled pump saturation parameter, b_0 is the optical thickness of the BEC at resonance and $n(x,t) = |\Psi(x,t)|^2$ is the local BEC density, which for a BEC of uniform density is normalised to $n(x,t) = 1$.

The backward field, B, at the BEC completes the feedback loop. As the field propagates a distance $2d$ from the BEC to the mirror and back, optical diffraction plays a critical role by converting phase modulations to amplitude modulations and consequently optical dipole forces. The relation between the Fourier components of the forward and backward fields at the BEC is

$$\tilde{B}(q) = \sqrt{R}\tilde{F}_{tr}(q)e^{-i\frac{q^2 d}{k_0}} \tag{3}$$

where R is the mirror reflectivity, q is the transverse wavenumber and $k_0 = \frac{2\pi}{\lambda_0}$.

3. Self-Structuring Instability

We now show that the BEC-SMF system exhibits a self-structuring instability where the optical fields and BEC density spontaneously develop spatially periodic modulations. To do this, we first rewrite Equation (1) in terms of a transformed wavefunction variable, $\psi = \Psi\exp(i\frac{\Delta s_0 \bar{t}}{4})$, where $s_0 = p_0(1+R)$, so that

$$i\frac{\partial\psi(\bar{x},\bar{t})}{\partial\bar{t}} = -\bar{\omega}_r\frac{\partial^2\psi}{\partial\bar{x}^2} + \frac{\Delta}{4}(s(\bar{x},\bar{t}) - s_0)\psi. \tag{4}$$

We now assume that the reflected optical field and the BEC wavefunction consist of a spatially uniform component and a small, time-dependent component which is also a function of the transverse coordinate, $\bar{x}$, so that

$$\psi(\bar{x},\bar{t}) = \psi_0 + \psi_1(\bar{x},\bar{t}) \tag{5}$$

$$B(\bar{x},\bar{t}) = B_0 + B_1(\bar{x},\bar{t}). \tag{6}$$

Consequently the BEC density and saturation parameter are

$$n(\bar{x},\bar{t}) = n_0 + n_1(\bar{x},\bar{t}) = 1 + \psi_0{\psi_1}^*(\bar{x},\bar{t}) + {\psi_0}^*\psi_1(\bar{x},\bar{t}) \tag{7}$$

$$s(\bar{x},\bar{t}) = s_0 + s_1(\bar{x},\bar{t}) = p_0(1+R) + B_0{B_1}^*(\bar{x},\bar{t}) + {B_0}^*B_1(\bar{x},\bar{t}) \tag{8}$$

where terms higher than first-order in time and space-dependent quantities have been neglected.

Substituting Equations (5) and (8) in Equation (4) gives

$$i\frac{\partial\psi_1(\bar{x},\bar{t})}{\partial\bar{t}} = -\bar{\omega}_r\frac{\partial^2\psi_1}{\partial\bar{x}^2} + \frac{\Delta}{4}(B_0{B_1}^*(\bar{x},\bar{t}) + {B_0}^*B_1(\bar{x},\bar{t}))\psi_0$$

which after Fourier transforming with respect to $\bar{x}$ becomes

$$i\frac{d\tilde{\psi}_1(\bar{q},\bar{t})}{d\bar{t}} = -\bar{\omega}_r\bar{q}^2\tilde{\psi}(\bar{q},\bar{t}) + \frac{\Delta}{4}\left(B_0\tilde{B}_1^*(\bar{q},\bar{t}) + {B_0}^*\tilde{B}_1(\bar{q},\bar{t})\right)\psi_0 \tag{9}$$

where $\bar{q} = \frac{q}{q_c}$ is a dimensionless transverse wavenumber. To calculate $\tilde{B}_1(\bar{q},\bar{t})$, we first find the optical field transmitted through the BEC, $F^{tr}(\bar{x},\bar{t})$ by substituting for $n(\bar{x},\bar{t})$ in Equation (2) using Equation(7), which results in

$$\begin{aligned} F^{tr}(\bar{x},\bar{t}) &= \sqrt{p_0}\exp\left(-i\frac{b_0}{2\Delta}(n_0 + n_1(x,t))\right) \\ &\approx {F^{tr}}_0 + {F^{tr}}_1(\bar{x},\bar{t}) \end{aligned} \tag{10}$$

where

$${F^{tr}}_0 = \sqrt{p_0}\exp\left(-i\frac{b_0}{2\Delta}\right) \tag{11}$$

$${F^{tr}}_1(\bar{x},\bar{t}) = -i\frac{b_0\sqrt{p_0}}{2\Delta}\exp\left(-i\frac{b_0}{2\Delta}\right)(\psi_0{\psi_1}^*(\bar{x},\bar{t}) + {\psi_0}^*\psi_1(\bar{x},\bar{t})) \tag{12}$$

We can now use this to calculate the reflected field using Equation (6), where

$$\begin{aligned} \tilde{F}^{tr}(\bar{q},\bar{t}) &= \frac{1}{2\pi}\int F^{tr}(\bar{x},\bar{t})e^{-i\bar{q}\bar{x}}\,d\bar{x} \\ &= \frac{1}{2\pi}\int \left({F^{tr}}_0 + {F^{tr}}_1(\bar{x},\bar{t})\right)e^{-i\bar{q}\bar{x}}\,d\bar{x} \\ &= {F^{tr}}_0\delta(\bar{q}) + \tilde{F}_1^{tr}(\bar{q},\bar{t}) \end{aligned} \tag{13}$$

and

$$\tilde{F}_1^{tr}(\bar{q},\bar{t}) = -i\frac{b_0\sqrt{p_0}}{2\Delta}\exp\left(-i\frac{b_0}{2\Delta}\right)(\psi_0\tilde{\psi}_1^*(\bar{q},\bar{t}) + {\psi_0}^*\tilde{\psi}_1(\bar{q},\bar{t})) \tag{14}$$

so from Equation (6)

$$\begin{aligned} \tilde{B}(\bar{q},\bar{t}) &= \sqrt{R}\tilde{F}^{tr}(\bar{q},\bar{t})\exp\left(-i\frac{\bar{q}^2\pi}{2}\right) \\ &= B_0\delta(\bar{q}) + \tilde{B}_1(\bar{q},\bar{t}) \end{aligned} \tag{15}$$

where

$$B_0 = \sqrt{R}{F^{tr}}_0 = \sqrt{Rp_0}\exp\left(-i\frac{b_0}{2\Delta}\right), \tag{16}$$

$$\begin{aligned} \tilde{B}_1(\bar{q},\bar{t}) &= \sqrt{R}\tilde{F}_1^{tr}(\bar{q},\bar{t}) \\ &= -i\frac{b_0\sqrt{p_0R}}{2\Delta}\exp\left(-i\frac{b_0}{2\Delta}\right)(\psi_0\tilde{\psi}_1^*(\bar{q},\bar{t}) + {\psi_0}^*\tilde{\psi}_1(\bar{q},\bar{t}))\exp\left(-i\frac{\bar{q}^2\pi}{2}\right). \end{aligned} \tag{17}$$

Substituting for $\tilde{B}_1(\bar{q},\bar{t})$ using Equation (17) in Equation (9) produces

$$i\frac{d\tilde{\psi}_1(\bar{q},\bar{t})}{d\bar{t}} = -\bar{\omega}_r\bar{q}^2\psi_1(\bar{q}) - \frac{Rp_0b_0\sin\left(\frac{\bar{q}^2\pi}{2}\right)}{4}(\psi_0\tilde{\psi}_1^*(\bar{q},\bar{t}) + {\psi_0}^*\tilde{\psi}_1(\bar{q},\bar{t}))\psi_0. \tag{18}$$

Fourier transforming Equation (7) and using Equation (18), the evolution of the Fourier component of the BEC density, $\tilde{n}_1(\bar{q},\bar{t})$ is described by

$$\frac{d^2\tilde{n}_1(\bar{q},\bar{t})}{d\bar{t}^2} = \left[\frac{\bar{\omega}_r\bar{q}^2b_0p_0R\sin\left(\frac{\bar{q}^2\pi}{2}\right)}{2} - \bar{\omega}_r^2\bar{q}^4\right]\tilde{n}_1(\bar{q},\bar{t}) \tag{19}$$

Assuming $\tilde{n}_1(\bar{q}\bar{t}) \propto \exp(\bar{g}\bar{t})$ then the instability threshold will occur when $\bar{g} = 0$, i.e., when the pump saturation parameter has the threshold value

$$p_0 = \frac{2\bar{\omega}_r\bar{q}^2}{b_0 R \sin\left(\frac{\bar{q}^2\pi}{2}\right)}. \tag{20}$$

Due to the periodicity of the sine function, this threshold will have multiple minima. The lowest threshold,

$$p_{th} = \frac{2\bar{\omega}_r\bar{q}^2}{b_0 R}, \tag{21}$$

occurs when $\bar{q} \approx 1$, i.e., $q = q_c$, as shown in Figure 2.

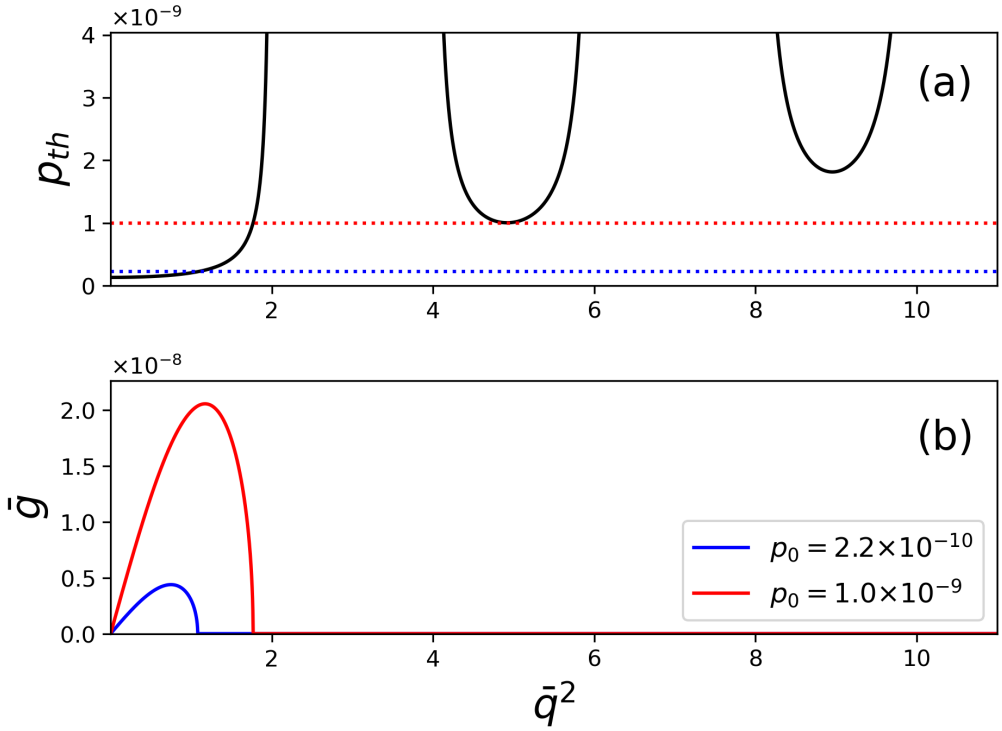


Figure 2. Plot of threshold pump saturation parameter (p_{th}) and growth rate ($\bar{g}$) against dimensionless transverse wavenumber squared, $\bar{q}^2$ as calculated from Equations (20) and (22). The dashed lines in (**a**) indicate the values of the pump saturation parameter, p_0, used in (**b**).

The dimensionless growth rate of the instability, $\bar{g}$, is

$$\bar{g} = \bar{\omega}_r\bar{q}^2\sqrt{\frac{p_0}{p_{th}} - 1} \tag{22}$$

The expressions for the threshold condition, Equation (20), and instability growth rate, Equation (22), were derived in [29] using an alternative approach. Note that the threshold in Equation (21) is independent of detuning, which implies that the real pump intensity will increase quadratically with detuning. The growth rate depends quadratically on the length scale selected by adjusting the mirror distance, d, and otherwise only on the distance to threshold.

The physical origin of the instability are BEC density modulations. As the BEC acts a refractive optical element, and the local refractive index of the BEC is proportional to its local density, density modulations result in refractive index modulations. The refractive index modulation with spatial frequency q_c produces a phase modulation in F_{tr} with spatial frequency q_c which is in turn converted into an intensity modulation of B (see Equation (3)) during the propagation and diffraction of the optical field between the BEC and the mirror

via the Talbot effect [33]. The intensity gradients produced by the intensity modulation in B then produce optical dipole forces which reinforce the density modulation, with spatial frequency q_c, resulting in positive feedback which leads to instability of the initial homogeneous state and results in BEC density and optical intensity modulations with spatial frequency q_c.

4. Self-Structuring Dynamics

In order to investigate the dynamical behaviour of the BEC-SMF system, we solve Equations (1)–(3) numerically for different pump saturation parameters (i.e., pump intensities). We consider the case where $\Delta = 500$, $\bar{\omega}_r = 1.00 \times 10^{-8}$, $b_0 = 100$ and $R = 0.99$. In these simulations, a small periodic density modulation with spatial period Λ_c is applied to the BEC density, i.e., $|\Psi(\bar{x}, \bar{t} = 0)| \propto (1 + \epsilon \cos(\bar{x}))$, where $\epsilon = 1 \times 10^{-6}$.

The character of the system evolution is dependent on how far the system is driven above threshold. As in [32], we consider two cases: weak driving, where the pump saturation parameter, p_0, marginally exceeds the threshold value p_{th} (i.e., $p_0 \approx p_{th}$), and strong driving, where p_0 significantly exceeds p_{th} (i.e., $p_0 \gg p_{th}$).

4.1. Weak Driving ($p_0 \approx p_{th}$)

Figure 3 shows the spatio-temporal evolution of the BEC density and optical saturation parameter (i.e., intensity) at the BEC when the pump saturation parameter $p_0 = 2.2 \times 10^{-10}$, which is slightly above the instability threshold (see blue dotted line in Figure 2a).

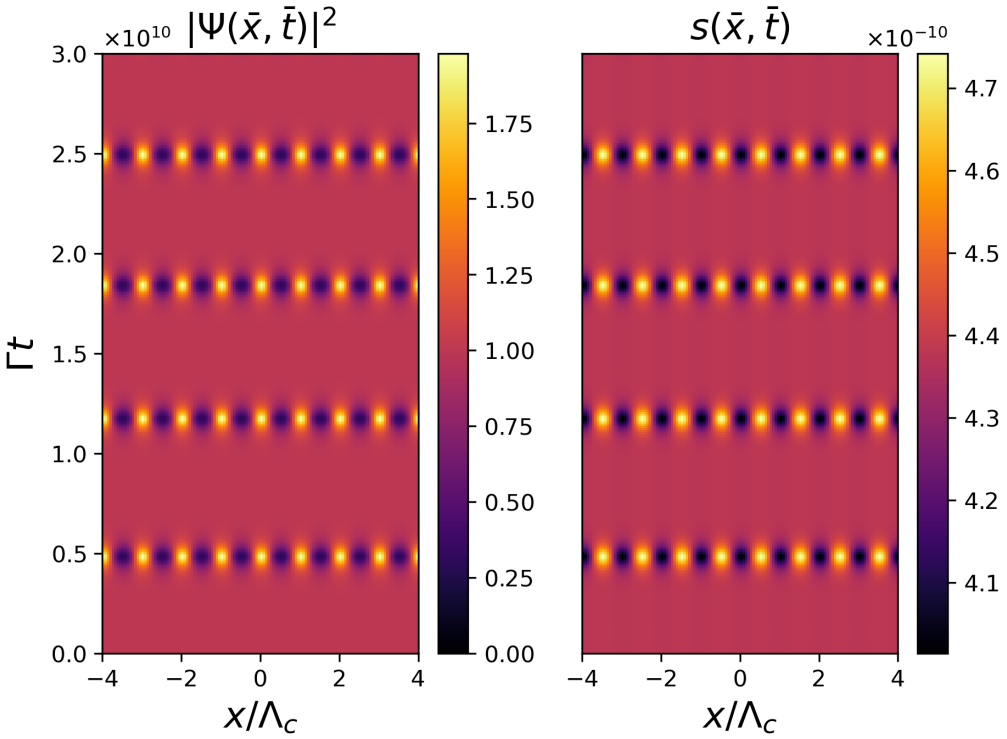


Figure 3. Spatio-temporal evolution of the BEC density and optical saturation parameter (i.e., intensity) at the BEC for a case of weak driving when the pump saturation parameter $p_0 = 2.2 \times 10^{-10}$.

It can be seen that the BEC density and optical intensity, both initially spatially homogeneous, spontaneously develop spatially periodic modulations with spatial period Λ_c. The maxima in atomic density lie at positions of minima in optical intensity. This is due to the fact that the interaction involves optical dipole forces and the pump field is blue-detuned from atomic resonance ($\Delta > 0$). For red-detuning ($\Delta < 0$), maxima of atomic density would lie on maxima of optical intensity [29]. The spatial width of the density and

intensity modulations are similar, with the intensity modulations being slightly wider due to the effect of diffraction as the field propagates between the BEC and the feedback mirror. Moreover, the system displays a temporal periodicity, oscillating between the spatially homogeneous state and the spatially periodic state. The system therefore behaves as a continuous space-time crystal, spontaneously developing spatial and temporal periodicity [34]. Figure 4 shows the temporal evolution of the BEC momentum distribution. It can be seen that the dynamics of the system involves only momentum states where $\bar{q} = 0, \pm 1$, i.e., with momentum $\hbar q = 0, \pm \hbar q_c$. The system evolves by periodically oscillating between 2 states: the state $\hbar q = 0$ (spatially homogeneous) and $\hbar q = \pm \hbar q_c$ i.e., $\cos(q_c x)$, spatially periodic [32]. An interesting feature of the BEC-SMF system is that the spatial period of the pattern (Λ_c) depends on the distance between the BEC and the mirror (d). The size of the patterns observed in Figure 3 can therefore be tuned by varying d. Consequently, the BEC-SMF system in the weak-driving regime offers the possibility of realising a continuous space-time crystal with a spatial period which is tunable rather than fixed as in [34].

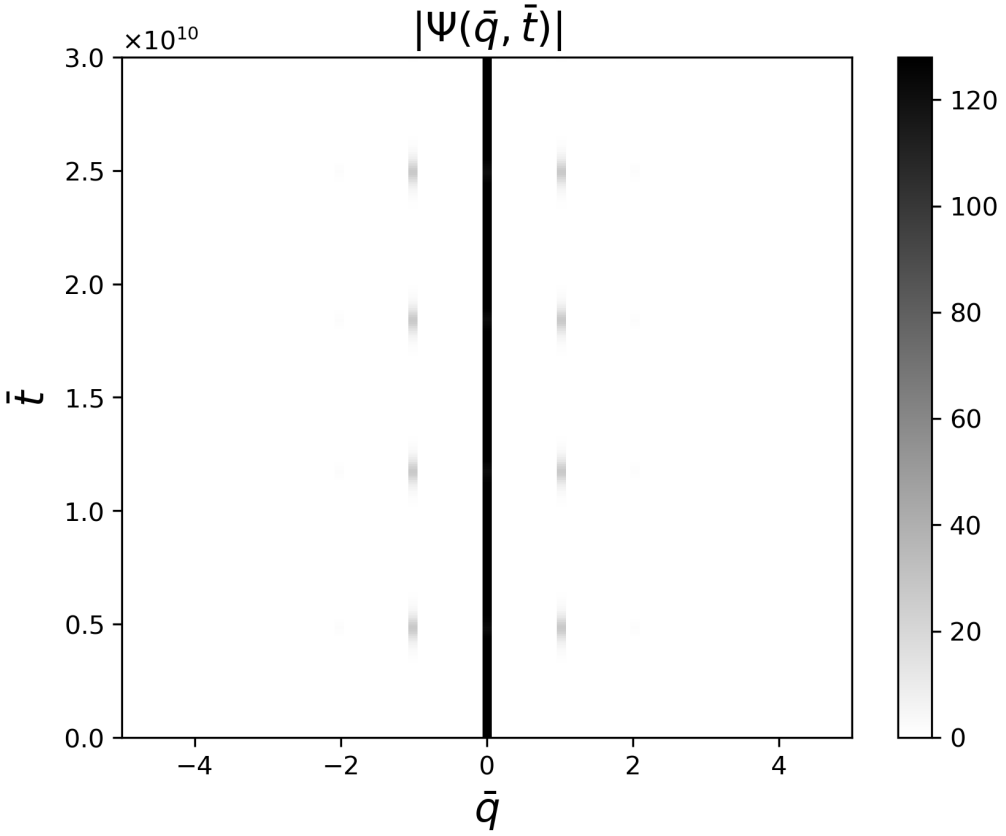


Figure 4. Evolution of the BEC momentum distribution for a case of weak driving where the pump saturation parameter $p_0 = 2.2 \times 10^{-10}$.

4.2. Strong Driving ($p_0 \gg p_{th}$)

Figure 5 shows the spatio-temporal evolution of the BEC density and optical saturation parameter (i.e., intensity) at the BEC when the pump saturation parameter $p_0 = 1.0 \times 10^{-9}$, which is significantly above the instability threshold (see red dotted line in Figure 2a). It can be seen that in this case the BEC density and optical intensity spontaneously develop more complex spatially periodic modulations or "chevrons" [35] with spatial period Λ_c which after their initial development display quasi-periodicity in time. The spatial distributions of the atomic density and optical intensity are again similar, with the maxima in atomic density lying at positions of minima in optical intensity. Diffractive spreading of modulations in optical intensity is more pronounced than in the weak driving regime (Figure 3) due to the

narrowness of the peaks in BEC density which form in the strong driving regime. Figure 6 shows the temporal evolution of the BEC momentum distribution in this case. It can be seen that the dynamics of the system now involves several different momentum states where $\bar{q} = 0, \pm 1, \pm 2, \pm 3 \ldots$.

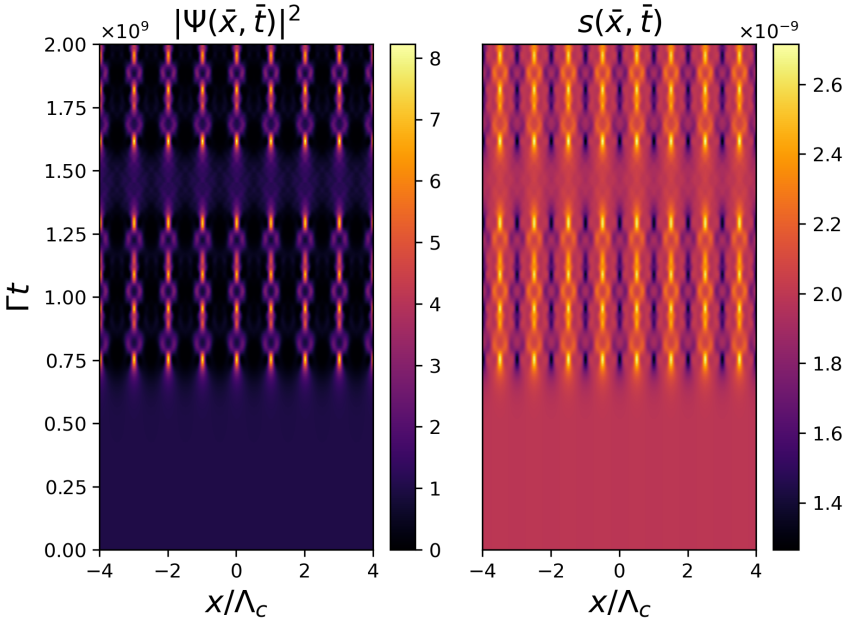


Figure 5. Spatio-temporal evolution of the BEC density and optical saturation parameter (i.e., intensity) at the BEC for a case of strong driving where when the pump saturation parameter $p_0 = 1.0 \times 10^{-9}$.

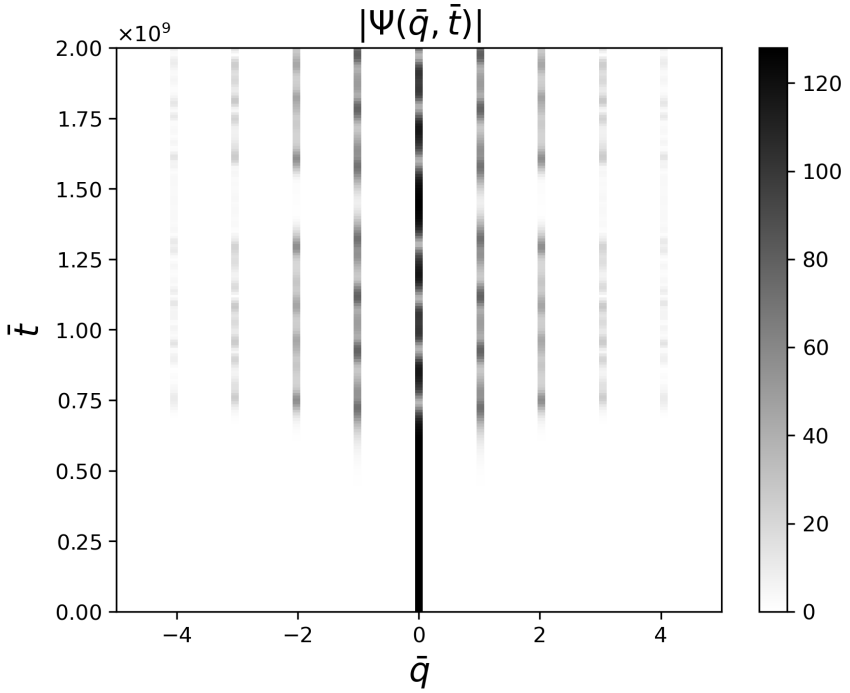


Figure 6. Evolution of the BEC momentum distribution for a case of strong driving where when the pump saturation parameter $p_0 = 1.0 \times 10^{-9}$.

In contrast to the case of weak driving, the dynamics in the case of strong driving cannot be described in terms of a two-state model [32].

Note from Figure 2 that if the pump saturation parameter, p_0, were to be increased above $p_0 = 1.0 \times 10^{-9}$ then a second instability "balloon" would develop around $\bar{q} = \sqrt{5}$,

followed by a third one around $\bar{q} = 3$. The evolution of the system is still dominated by the patterns with the lowest threshold around $\bar{q} \approx 1$ but in general will become more complex and sensitive to initial conditions. A full analysis of this scenario will be the subject of a separate study.

A useful measure of the degree of spatial modulation in the BEC is the magnitude of the Fourier component of the BEC density at spatial frequency q_c, i.e.,

$$n_{q_c}(\bar{t}) = \frac{1}{\bar{L}} \int_{-\frac{\bar{L}}{2}}^{\frac{\bar{L}}{2}} |\psi(\bar{x}, \bar{t})|^2 \, \exp(i\bar{x}) \, d\bar{x} \tag{23}$$

where $\bar{L}$ is the length of the domain in the simulation. Figure 7 shows the evolution of $|n_{q_c}|$ when $p_0 = 2.2 \times 10^{-10}$ and $p_0 = 1.0 \times 10^{-9}$, corresponding to Figure 3 and Figure 5, respectively. It can be seen from Figure 7a that in the weak driving regime, $|n_{q_c}|$ oscillates periodically in time, whereas from Figure 7b, in the weak driving regime $|n_{q_c}|$ grows exponentially before performing quasi-periodic oscillations.

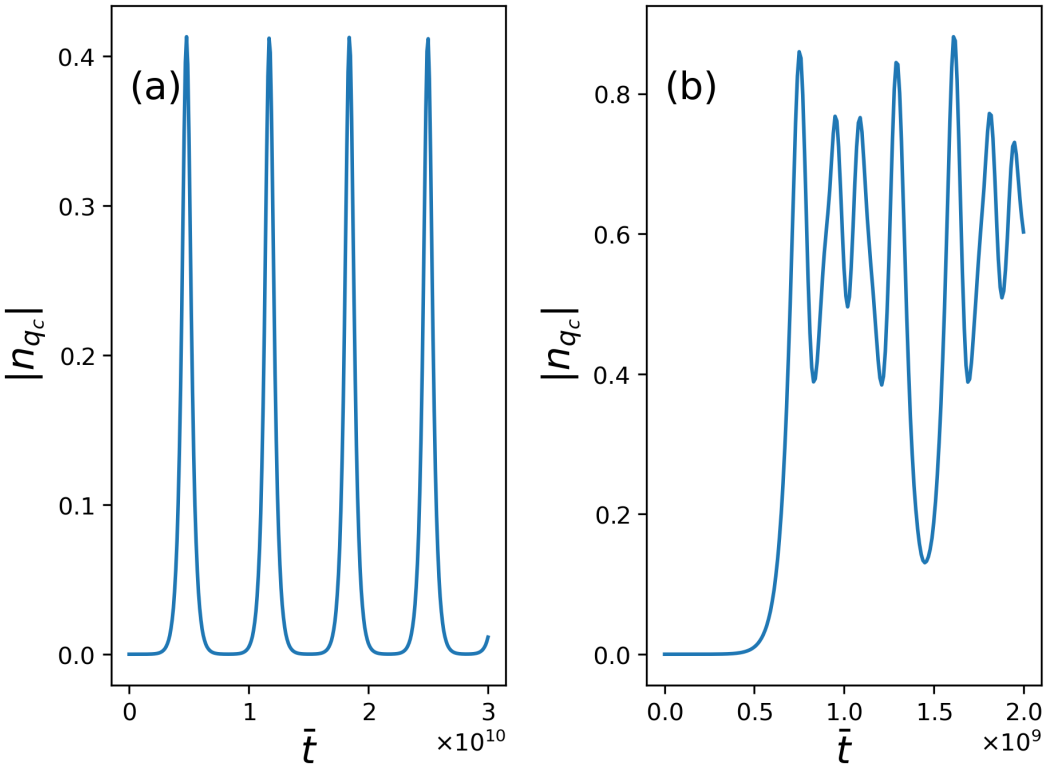


Figure 7. Plot of $|n_{q_c}|$ against $\bar{t}$ when (**a**) $p_0 = 2.2 \times 10^{-10}$, (**b**) $p_0 = 1.0 \times 10^{-9}$.

In [32], it was shown that the BEC-SMF model could be mapped onto the quantum HMF model. A consequence of this is that in the weak-driving limit, assuming that $n(\bar{x}, \bar{t})$ is spatially periodic with period 2π in $\bar{x}$ (period Λ_c in x), then $|n_{q_c}|$ can be expressed analytically as

$$|n_{q_c}(\bar{t})| = \sqrt{2}\frac{p_{th}}{p_0}\sqrt{\frac{p_0}{p_{th}} - 1}\,\mathrm{sech}\left[\bar{\omega}_r\sqrt{\frac{p_0}{p_{th}} - 1}(\bar{t} - \bar{t}_0)\right] \tag{24}$$

where

$$\bar{t}_0 = \frac{\cosh^{-1}\left(\frac{\sqrt{2}\frac{p_{th}}{p_0}\sqrt{\frac{p_0}{p_{th}} - 1}}{|n_{q_c}^{(0)}|}\right)}{\bar{\omega}_r\sqrt{\frac{p_0}{p_{th}} - 1}}. \tag{25}$$

and $n_{q_c}^{(0)} = n_{q_c}(\bar{t} = 0)$. Equation (24) describes each oscillation period of $|n_{q_c}|$ shown in Figure 7a [32].

Figure 8 shows the maximum value of $|n_{q_c}|$ plotted against p_0. It can be seen that the maximum value of $|n_{q_c}|$ scales with distance from threshold $\propto (p_0 - p_{th})^{1/2}$, similar to the mean-field Ising model [36]. The figure shows that for p_0 values just above threshold, where the weak-driving limit applies and the interaction involves only 2 spatial modes, the value of $|n_{q_c}|_{max}$ is in good agreement with the value predicted by the analytical expression Equation (24). As p_0 increases, the agreement between the simulation results and that predicted by Equation (24) begin to diverge as the system is driven more strongly, with more spatial modes participating in the interaction and the assumptions made in deriving Equation (24) becoming invalid.

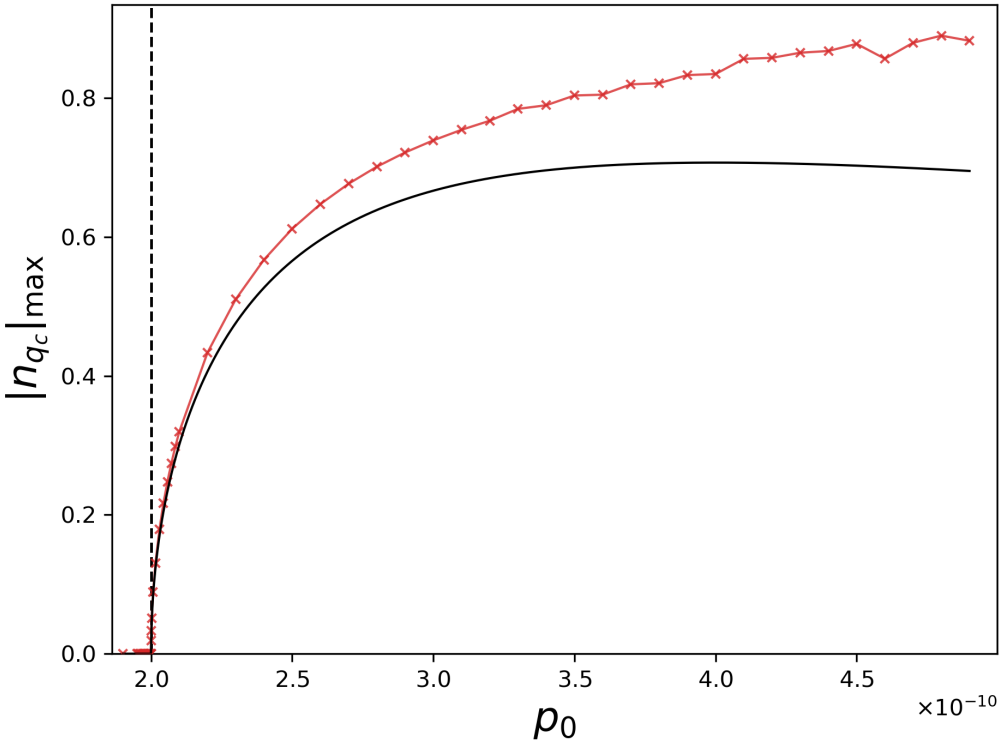


Figure 8. Maximum density modulation amplitude, $|n_{q_c}|_{\max}$ versus pump saturation parameter p_0. Red crosses: Maximum magnitude of the first-harmonic density component, $|n(q_c)|$ calculated from simulations [cf. Equation (23)]. Black solid line: analytic prediction for $|n_{q_c}|_{\max}$ from the two-mode (first-harmonic) theory, $|n_{q_c}(t_0)|$. The vertical dashed line indicates the instability threshold $p_0 = p_{\text{th}}$ (Equation (21)).

As the linear growth rate of the instability also depends on pump saturation parameter, p_0 (see Equation (22)), then the time for the spatial modulation amplitude, $|n_{q_c}|$, to reach its maximum value will also depend on p_0. Figure 9 shows the dependence of the delay time, $\bar{t}_D$, i.e., the time required for $|n_{q_c}|$ to grow to $|n_{q_c}|_{\max}$, on p_0. It shows that the values of $\bar{t}_D$ from the simulations agree well with the analytical expression in Equation (25). Although Equation (25) was derived assuming weak driving, with only two spatial modes participate in the interaction, Figure 9 shows that it also provides an accurate prediction of $\bar{t}_D$ significantly above threshold.

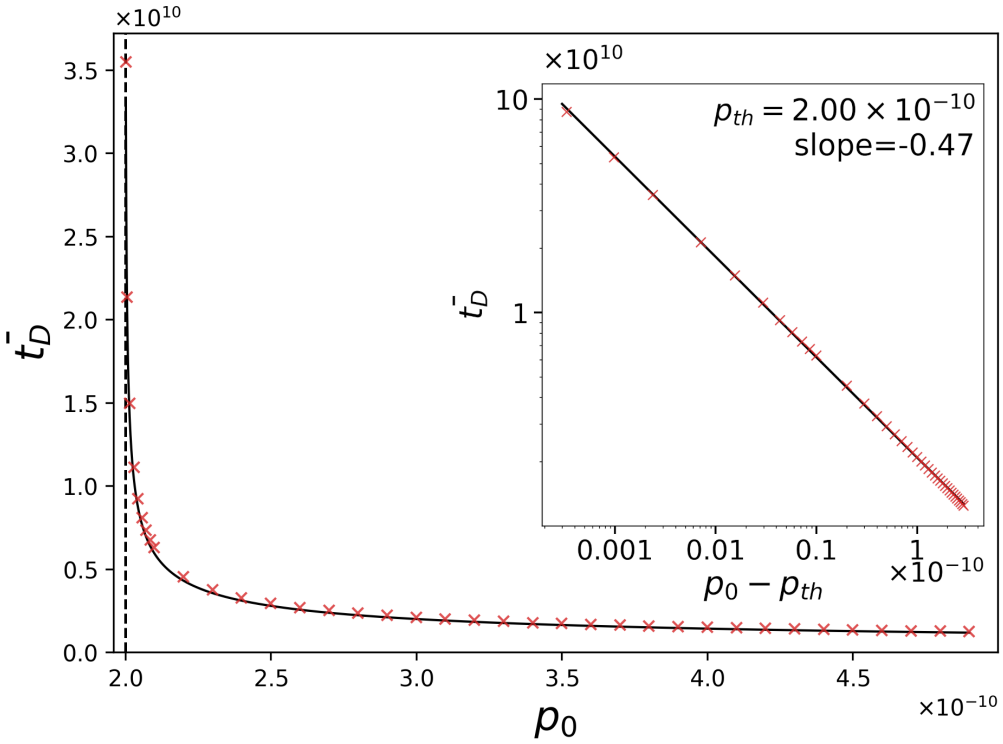


Figure 9. Delay time, $\bar{t}_D$ versus pump saturation parameter p_0. Red crosses: delay times $\bar{t}_D$ extracted from numerical simulations, defined as the time taken for the density modulation amplitude, $|n_{q_c}|$, to reach its maximum value. Black solid line: analytical prediction for the delay time, $\bar{t}_0$, from Equation (25). The vertical dashed line indicates the instability threshold $p_0 = p_{\text{th}}$. Inset: log–log plot of $\bar{t}_D$, versus $p_0 - p_{\text{th}}$. The threshold p_{th} is determined by scanning p_{th} and selecting the value that minimises the residual sum of squares of a linear fit in log–log space. The resulting fit yields a slope -0.4740 ± 0.0006 and threshold $p_{\text{th}} = (2.00 \pm 0.02) \times 10^{-10}$, with uncertainties obtained from the fit covariance.

5. Conclusions

We have studied a 1D model of a diffraction-mediated self-structuring instability which can occur when a BEC is illuminated by a pump laser and its reflection from a single feedback mirror. We performed a linear stability analysis of the model and derived expressions for the threshold value of the pump saturation parameter and the instability growth rate. Using numerical simulation of the BEC-SFM system, we investigated the dynamics of the self-structuring and demonstrated the existence of two different regimes: weak driving and strong driving. For weak driving, the system behaves as a continuous space-time crystal oscillating between two states (spatially uniform and periodic), whereas for strong driving, many BEC momentum states are excited and the BEC density develops chevrons which form and disperse quasi-periodically. Our simulations showed the dependence of the pattern modulation depth and pattern formation time on pump saturation parameter, p_0. We compared these simulation results with analytical expressions derived from the quantum HMF model in the weak driving regime [32]. We found excellent agreement in the dependence of pattern modulation depth on p_0 for the case of weak driving, and in the dependence of pattern formation time on p_0 for both weak driving and strong driving. The results presented show that the BEC-SMF system offers a route to the first experimental realisation of the quantum Hamiltonian Mean Field model, one of the fundamental models involving long-range coupling in statistical physics [32], and of a continuous space-time crystal with a tunable spatial period.

Extending the model presented here to two spatial dimensions will allow a wider range of pattern geometries and structures to be investigated [30,31].

Author Contributions: Simulations—G.R.M.R. and K.O.; Analysis—G.R.M.R., K.O., G.-L.O. and T.A.; Writing, reviewing and editing—G.R.M.R., K.O., G.-L.O. and T.A. All authors have read and agreed to the published version of the manuscript.

Funding: This research was funded by the Engineering & Physical Sciences Research Council (EPSRC) via grant number UKRI 2897. K.O-D. is supported by the EPSRC Centre for Doctoral Training in Applied Quantum Technologies (CDT-AQT).

Data Availability Statement: All data underpinning this publication are openly available from the University of Strathclyde KnowledgeBase at https://doi.org/10.15129/251cc418-b54a-4f70-8b5f-be62484f32ce, accessed on 8 April 2026 .

Conflicts of Interest: The authors declare no conflicts of interest.

References

1. Cross, M.C.; Hohenberg, P.C. Pattern formation outside of equilibrium. *Rev. Mod. Phys.* **1993**, *65*, 851. [CrossRef]
2. Grynberg, G.; Le Bihan, E.; Verkerk, P.; Simoneau, P.; Leite, J.R.; Bloch, D.; Le Boiteux, S.; Ducloy, M. Observation of instabilities due to mirrorless four-wave mixing oscillation in sodium. *Opt. Commun.* **1988**, *67*, 363–366. [CrossRef]
3. Lippi, G.; Ackemann, T.; Hoffer, L.; Lange, W. Transverse structures in a sodium-filled Fabry-Pérot resonator—I. Experimental results: Symmetries and the role of the incoupling conditions. *Chaos Solitons Fractals* **1994**, *4*, 1409–1431. [CrossRef]
4. Lippi, G.; Ackemann, T.; Hoffer, L.; Lange, W. Transverse structures in a sodium-filled Fabry-Pérot resonator—II. Interpretation of experimental results. *Chaos Solitons Fractals* **1994**, *4*, 1433–1449. [CrossRef]
5. Giusfredi, G.; Valley, J.; Pon, R.; Khitrova, G.; Gibbs, H. Optical instabilities in sodium vapor. *J. Opt. Soc. Am. B* **1988**, *5*, 1181–1192. [CrossRef]
6. Firth, W. Spatial instabilities in a Kerr medium with single feedback mirror. *J. Mod. Opt.* **1990**, *37*, 151–153. [CrossRef]
7. Arecchi, F.T.; Boccaletti, S.; Ramazza, P.L. Pattern formation and competition in nonlinear optics. *Phys. Rep.* **1999**, *318*, 1–83. [CrossRef]
8. Lugiato, L.A. Transverse nonlinear optics: Introduction and review (Editorial to special issue: Nonlinear optical structures, patterns, chaos). *Chaos Solitons Fractals* **1994**, *4*, 1251–1258. [CrossRef]
9. Rosanov, N.N. Transverse patterns in wide-aperture nonlinear optical systems. In *Progress in Optics*; Elsevier: Amsterdam, The Netherlands, 1996; Volume XXXV, pp. 1–60.
10. Barbay, S.; Kuszelewicz, R.; Tredicce, J.R. Cavity Solitons in VCSEL Devices. *Adv. Opt. Technol.* **2011**, *2011*, 628761. [CrossRef]
11. Grynberg, G.; Maître, A.; Petrossian, A. Flowerlike patterns generated by a laser beam transmitted through a rubidium cell with a single feedback mirror. *Phys. Rev. Lett.* **1994**, *72*, 2379–2382. [CrossRef]
12. Ackemann, T.; Lange, W. Non- and nearly hexagonal patterns in sodium vapor generated by single-mirror feedback. *Phys. Rev. A* **1994**, *50*, R4468–R4471. [CrossRef]
13. Ackemann, T.; Lange, W. Optical pattern formation in alkali metal vapors: Mechanisms, phenomena and use. *Appl. Phys. B* **2001**, *72*, 21–34. [CrossRef]
14. Greenberg, J.A.; Schmittberger, B.L.; Gauthier, D. Bunching-induced optical nonlinearity and instability in cold atoms. *Opt. Exp.* **2011**, *19*, 22535. [CrossRef] [PubMed]
15. Schmittberger, B.L.; Gauthier, D.J. Spontaneous emergence of free-space optical and atomic patterns. *New J. Phys.* **2016**, *18*, 10302. [CrossRef]
16. Kruse, D.; von Cube, C.; Zimmermann, C.; Courteille, P.W. Observation of lasing mediated by collective atomic recoil. *Phys. Rev. Lett.* **2003**, *91*, 183601. [CrossRef]
17. Ritsch, H.; Domokos, P.; Brennecke, F.; Esslinger, T. Cold atoms in cavity-generated dynamical optical potentials. *Rev. Mod. Phys.* **2013**, *85*, 553–601. [CrossRef]
18. Mivehvar, F.; Piazza, F.; Donner, T.; Ritsch, H. Cavity QED with quantum gases: New paradigms in many-body physics. *Adv. Phys.* **2021**, *70*, 1–153. [CrossRef]
19. Kollar, A.J.; Papageorge, A.T.; Vaidya, V.D.; Guo, Y.; Keeling, J.; Lev, B.L. Supermode-density-wave-polariton condensation with a Bose–Einstein condensate in a multimode cavity. *Nat. Commun.* **2017**, *8*, 14386. [CrossRef]
20. Kroeze, R.M.; Guo, Y.; Vaidya, V.D.; Keeling, J.; Lev, B.L. Spinor self-ordering of a quantum gas in a cavity. *Phys. Rev. Lett.* **2018**, *121*, 163601. [CrossRef]
21. Guo, Y.; Kroeze, R.M.; Marsh, B.P.; Gopalakrishnan, S.; Keeling, J.; Lev, B.L. An optical lattice with sound. *Nature* **2021**, *599*, 211. [CrossRef]
22. Robb, G.; Piovella, N.; Ferraro, A.; Bonifacio, R.; Courteille, P.W.; Zimmermann, C. Collective atomic recoil lasing including friction and diffusion effects. *Phys. Rev. A* **2004**, *69*, 041403. [CrossRef]

23. Baumann, K.; Guerlin, C.; Brennecke, F.; Esslinger, T. Dicke quantum phase transition with a superfluid gas in an optical cavity. *Nature* **2010**, *464*, 1301–1306. [CrossRef] [PubMed]
24. Mottl, R.; Brennecke, F.; Baumann, K.; Landig, R.; Donner, T.; Esslinger, T. Roton-type mode softening in a quantum gas with cavity-mediated long-range interactions. *Science* **2012**, *336*, 1570–1573. [CrossRef] [PubMed]
25. Schuster, S.; Wolf, P.; Ostermann, S.; Slama, S.; Zimmermann, C. Supersolid properties of a Bose-Einstein condensate in a ring resonator. *Phys. Rev. Lett.* **2020**, *124*, 143602. [CrossRef]
26. Léonard, J.; Morales, A.; Zupancic, P.; Esslinger, T.; Donner, T. Supersolid formation in a quantum gas breaking a continuous translational symmetry. *Nature* **2017**, *543*, 87–90. [CrossRef]
27. Labeyrie, G.; Tesio, E.; Gomes, P.M.; Oppo, G.L.; Firth, W.J.; Robb, G.R.; Arnold, A.S.; Kaiser, R.; Ackemann, T. Optomechanical self-structuring in a cold atomic gas. *Nat. Photonics* **2014**, *8*, 321–325. [CrossRef]
28. Tesio, E. Theory of Self-Organisation in Cold Atoms. Ph.D. Thesis, University of Strathclyde, Glasgow, UK, 2014.
29. Robb, G.; Tesio, E.; Oppo, G.L.; Firth, W.; Ackemann, T.; Bonifacio, R. Quantum threshold for optomechanical self-structuring in a Bose-Einstein condensate. *Phys. Rev. Lett.* **2015**, *114*, 173903. [CrossRef]
30. Zhang, Y.C.; Walther, V.; Pohl, T. Long-range interactions and symmetry breaking in quantum gases through optical feedback. *Phys. Rev. Lett.* **2018**, *121*, 073604. [CrossRef]
31. Zhang, Y.C.; Walther, V.; Pohl, T. Self-bound droplet clusters in laser-driven Bose-Einstein condensates. *Phys. Rev. A* **2021**, *103*, 023308. [CrossRef]
32. Robb, G.; Walker, J.; Oppo, G.L.; Ackemann, T. Long-range interactions in a quantum gas mediated by diffracted light. *Phys. Rev. Res.* **2023**, *5*, L032004. [CrossRef]
33. Talbot, H.I. Facts relating to optical science. No. III. *London Edinburgh Dublin Philos. Mag. J. Sci.* **1836**, *9*, 1–4. [CrossRef]
34. Zhao, H.; Smalyukh, I. Space-time crystals from particle-like topological solitons. *Nat. Mater.* **2025**, *24*, 1802–1811. [CrossRef]
35. Plestid, R.; Mahon, P.; O'Dell, D.H.J. Violent relaxation in quantum fluids with long-range interactions. *Phys. Rev. E* **2018**, *98*, 012112. [CrossRef]
36. Als-Nielsen, J.; Birgeneau, R.J. Mean field theory, the Ginzburg criterion, and marginal dimensionality of phase transitions. *Am. J. Phys.* **1977**, *45*, 554–560. [CrossRef]

Disclaimer/Publisher's Note: The statements, opinions and data contained in all publications are solely those of the individual author(s) and contributor(s) and not of MDPI and/or the editor(s). MDPI and/or the editor(s) disclaim responsibility for any injury to people or property resulting from any ideas, methods, instructions or products referred to in the content.